Journal of Solid Mechanics Vol. 4, No. 1 (2012) pp. 1-14

Nonlinear Vibration of Smart Micro-Tube Conveying Fluid Under Electro-Thermal Fields

A. Ghorbanpour Arani[1,2*], E. Haghparast[1], S. Amir[1]

[1]*Faculty of Mechanical Engineering, University of Kashan, Kashan, Islamic Republic of Iran*
[2]*Institute of Nanoscience & Nanotechnology, University of Kashan, Kashan, Islamic Republic of Iran*

Received 2 November 2011; accepted 4 January 2012

ABSTRACT
In this study, electro-thermo-mechanical nonlinear vibration and instability of embedded piezoelectric micro-tube is carried out based on nonlocal theory and nonlinear Donnell's shell model. The smart micro-tube made of Poly-vinylidene fluoride (PVDF) is conveying an isentropic, incompressible fluid. The detailed parametric study is conducted, focusing on the remarkable effects of mean flow velocity, fluid viscosity, elastic medium modulus, temperature change, imposed electric potential, small scale and aspect ratio on the vibration behavior of the micro-tube. It has been found that stability of the system is strongly dependent on the imposed electric potential. Results of this investigation could be applied for optimum design of sensors and actuators in the sensitive applications.

Keywords: Nonlinear vibration; Nonlocal theory; Smart structure; Conveying fluid; shell model

1 INTRODUCTION

MICRO-TUBES are the core structures widely used in the micro/nano-electro-mechanical systems (MEMS/NEMS) and atomic force microscopes. These structures are often subjected to severe thermal environments during manufacturing and working, and thus the thermal effects become a primary design factor in specific cases. With the development of the material science, micro–electro-mechanical systems are the new field in which piezoelectric materials have been utilized to achieve the desired performance.

In recent years, various investigations have been carried out to study the buckling, dynamic stability, and free vibration of the smart structures in which the shell theory have been employed. Salehi-Khojin and Jalili [1] studied the buckling behavior of boron nitride nano-tube (BNNT) reinforced PVDF under combined electro-thermo-mechanical loadings considering the effect of piezoelectric property of BNNT. Their results show that applying direct and reverse voltages to BNNT changes the buckling loads for any axial and circumferential wave numbers. Recently, based on nonlocal piezoelasticity theory, vibration and buckling behavior of DWBNNTs embedded in an elastic medium with and without fluid was studied by Ghorbanpour Arani et al. [2-4]. They showed that the electric field effect on the frequency is approximately constant, while it decreases with increasing temperature change. Also, they concluded that the electric field and its direction have affected the magnitude of the critical buckling load.

Using generalized differential quadrature method, Shu [5] investigated free vibration of composite conical shell reinforced with a piezoelectric layer. Free vibration response of composite sandwich cylindrical shell with flexible core is studied by Rahmani et al. [6]. Their results revealed that the sandwich shells with flexible core exhibit a complex behavior, and that the vibration patterns of the sandwich cylindrical shells are more complex than

*Corresponding author. Tel.: +98 55912450; Fax: +98 361 55912424.
E-mail address: aghorban@kashanu.ac.ir (A.Ghorbanpour Arani).

those of the homogeneous shells. Furthermore, it was observed that the natural modes of the sandwich shell are different from those of the sandwich plate and have a mixed mode nature.

Flow induced vibration and fluid instability of tubular pipe and shell has been developed in other pervious literatures. Amabili et al. [7] on the other hand considered the tube as a cylindrical circular shell and therefore they were able to obtain a three-dimensional model for fluid flow. Ghorbanpour Arani et al. [8] investigated the nonlinear vibration and stability analysis of a polymeric composite smart micro-tube reinforced by BNNT. They found that stability of the micro-tube is strongly dependent on imposed electric potential, where increasing the imposed positive electric potential significantly increases the stability of the system. Also, their results showed using BNNTs as a piezoelectric fiber and its orientation angle with respect to micro-tube axis have significant effects on the vibration response and stability of the system.

Motivated by these considerations, the need for investigation of nonlinear vibration and stability of a smart piezoelectric micro-tube made of PVDF conveying fluid is very much felt, where it has not been found in the literature. Moreover, several effects of fluid flow on the vibration behavior of the micro-tube are investigated thoroughly as well as effect of other parameters such as small scale, temperature change, fluid viscosity, electric potential and elastic medium modulus.

2 ELECTRO-THERMAL ANALYZING

A schematic diagram of an embedded piezoelectric micro-tube conveying viscous fluid subjected to applied voltage is shown in Fig. 1.

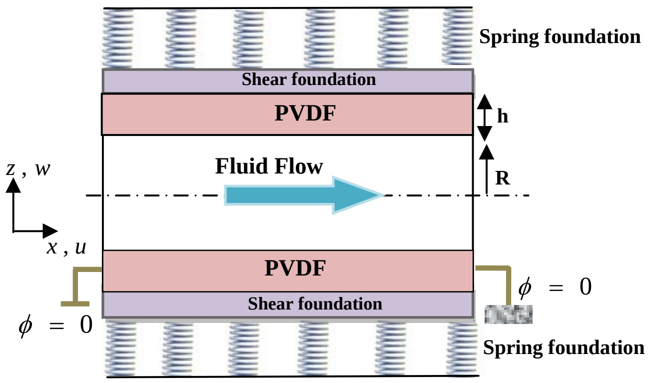

Fig.1
Configurations of the PVDF micro-tube conveying fluid.

Assuming plane stress condition and unidirectional electric field along the micro-tube, the constitutive equations for the electro-thermo-mechanical behavior of piezoelectric smart structures are expressed as [8]:

$$\begin{Bmatrix} \sigma_{xx} \\ \sigma_{\theta\theta} \\ \tau_{x\theta} \\ D_x \end{Bmatrix} = \begin{bmatrix} C_{xxxx} & C_{xx\theta\theta} & 0 & -e_{xxx} \\ C_{xx\theta\theta} & C_{\theta\theta\theta\theta} & 0 & -e_{x\theta\theta} \\ 0 & 0 & C_{x\theta x\theta} & 0 \\ e_{xxx} & e_{x\theta\theta} & 0 & \in_x \end{bmatrix} \begin{Bmatrix} \varepsilon_{xx} \\ \varepsilon_{\theta\theta} \\ \gamma_{x\theta} \\ E_x \end{Bmatrix} - \begin{Bmatrix} \lambda_{xx} \\ \lambda_{\theta\theta} \\ \lambda_{x\theta} \\ p_x \end{Bmatrix} \Delta\Theta \tag{1}$$

where $\{\sigma\}$, $\{\varepsilon\}$, $\{D\}$ and $\{E\}$ are stress, strain, electric displacement and electric field vectors respectively and $[C]$, $[e]$ and $[\in]$ are matrices of elastic stiffness, piezoelectric and dielectric constants respectively. Furthermore, the coefficients of thermal expansion, pyroelectric and temperature change are shown by $\{\lambda\}$, $\{p\}$ and $\Delta\Theta$ respectively and x, θ and z are longitudinal, circumferential and transverse coordinates with the origin located at the mid-plane of the micro-tube.

The longitudinal component of electric field in terms of electric potential is defined as [9]:

$$E_x = -\frac{\partial \phi}{\partial x} \tag{2}$$

where ϕ denotes the scalar function of electric potential.

According to the Eringen's nonlocal elasticity model [10], the stress state at a reference point in the body is regarded to be dependent not only on the strain state at this point but also on the strain states at all of the points throughout the body. On the other contract, at the local elasticity theory, the stress state at any point corresponds to the strain state at this point. The constitutive equations of the nonlocal elasticity can be considered as:

$$\left(1-(e_0 a)^2 \nabla^2\right)\{\sigma\}_{nonlocal} = \{\sigma\}_{classical} \tag{3}$$

where $e_0 a$ is a constant parameter showing the small scale effect and operator ∇^2 is defined as $\frac{\partial^2}{\partial x^2}+\frac{1}{R^2}\frac{\partial^2}{\partial \theta^2}$.

Eq. (3) is implicit relation between nonlocal and classical stresses.

3 FUNDAMENTAL FORMULATIONS

3.1 Strain displacement relationships

Based on shell model, the displacement components of an arbitrary point along x, θ and z coordinates are denoted by $\tilde{U}$, $\tilde{V}$ and $\tilde{W}$, respectively, which are expressed in the following form [11]:

$$\begin{aligned}
\tilde{U}(x,\theta,z,t) &= u(x,\theta,t) - z\frac{\partial w(x,\theta,t)}{\partial x}\\
\tilde{V}(x,\theta,z,t) &= v(x,\theta,t) - z\frac{1}{R}\frac{\partial w(x,\theta,t)}{\partial \theta}\\
\tilde{W}(x,\theta,z,t) &= w(x,\theta,t)
\end{aligned} \tag{4}$$

where u, v and w are components of the tube mid-plane displacement and t is the time.

According to Donnell's nonlinear shell theory the strain-displacement relations can be written as [11]:

$$\begin{aligned}
\varepsilon_x &= \frac{\partial u}{\partial x} + \frac{1}{2}\left(\frac{\partial w}{\partial x}\right)^2 - z\frac{\partial^2 w}{\partial x^2}\\
\varepsilon_\theta &= \frac{1}{R}\frac{\partial v}{\partial \theta} + \frac{w}{R} + \frac{1}{2}\left(\frac{1}{R}\frac{\partial w}{\partial \theta}\right)^2 - z\frac{1}{R^2}\frac{\partial^2 w}{\partial \theta^2}\\
\gamma_{x\theta} &= \frac{1}{R}\frac{\partial u}{\partial \theta} + \frac{\partial v}{\partial x} + \frac{1}{R}\frac{\partial w}{\partial x}\frac{\partial w}{\partial \theta} - 2z\frac{1}{R}\frac{\partial^2 w}{\partial x \partial \theta}
\end{aligned} \tag{5}$$

3.2 Energies of the smart micro-tube

The total potential energy of the smart micro-tube considering the potential of the electric field, is defined as [9]:

$$U_S = \frac{1}{2}\iiint_{\forall}\left(\varepsilon^T \sigma - E^T D\right) d\forall \tag{6}$$

where $\forall$ represents volume of the micro-tube which is dependent on thickness h and mean radius R as shown in Fig.1.

The kinetic energy of a cylindrical shell is expressed as [11]:

$$T_S = \frac{1}{2}\rho_s \iiint_{\forall} \vec{V}.\vec{V} d\forall \tag{7}$$

where ρ_s and $\vec{V}$ are density and velocity vector of the shell, respectively.

The kinetic energy of the micro-tube by neglecting rotary inertia and retaining in-plane inertia can be written as:

$$T_S = \frac{1}{2}\rho_s \int_0^{2\pi}\int_0^{L}\int_{-h/2}^{h/2}\left[\left(\frac{\partial u}{\partial t}\right)^2 + \left(\frac{\partial v}{\partial t}\right)^2 + \left(\frac{\partial w}{\partial t}\right)^2\right] dzdxRd\theta \tag{8}$$

The surrounding media of the micro-tube is modeled by Pasternak foundation based on which the external work is introduced as [12]:

$$W^{Elastic\ medium} = -\frac{1}{2}\int_0^{2\pi}\int_0^{L}\left(K_w w - G_p \nabla^2 w\right) w dxRd\theta \tag{9}$$

where K_w and G_p are Winkler spring and Pasternak shear modulus, respectively.

3.3 Mode expansion of displacements and electric potential

According to the simply supported boundary conditions of the micro-tube at two ends, the following mode expansion for components of displacement can be presented [13]:

$$\begin{aligned}
u &= \sum_{m=1}^{M}\sum_{n=0}^{N}\sin\left(\frac{(2m-1)\pi x}{L}\right)\left[U_{mn}^{c}(t)\cos(n\theta) + U_{mn}^{s}(t)\sin(n\theta)\right] \\
v &= \sum_{m=1}^{M}\sum_{n=0}^{N}\sin\left(\frac{(2m-1)\pi x}{L}\right)\left[V_{mn}^{c}(t)\cos(n\theta) + V_{mn}^{s}(t)\sin(n\theta)\right] \\
w &= \sum_{m=1}^{M}\sum_{n=0}^{N}\sin\left(\frac{(2m-1)\pi x}{L}\right)\left[W_{mn}^{c}(t)\cos(n\theta) + W_{mn}^{s}(t)\sin(n\theta)\right]
\end{aligned} \tag{10}$$

where m and n are longitudinal half wave number and circumferential wave number, respectively, M and N are maximum value of wave numbers. $U_{mn}^{c}(t)$, $U_{mn}^{s}(t)$, $V_{mn}^{c}(t)$, $V_{mn}^{s}(t)$, $W_{mn}^{c}(t)$ and $W_{mn}^{s}(t)$ are time-dependent degrees of freedom (DOFs) and $\{q_d\} = \left[U_{mn}^{c}, U_{mn}^{s}, V_{mn}^{c}, V_{mn}^{s}, W_{mn}^{c}, W_{mn}^{s}\right]^T$ is the vector of DOFs. The vector dimension of $\{q_d\}$ denotes number of DOFs which may be calculated as $N^{DOF} = 3\times(2M \times N + M)$.

For electric potential ϕ, the following mode expansion can be proposed [14]:

$$\phi = \phi_0\left(1 - \frac{x}{L}\right) + \sum_{m=1}^{M}\phi_m^s \sin\left(\frac{(2m-1)\pi x}{L}\right) \tag{11}$$

where ϕ_m^s is the time-independent amplitude component of electric potential and $\{q_\phi\} = \left[\phi_m^s\right]^T$ is defined as amplitudes of electric potential vector and ϕ_0 denote the imposed electric potential.

Due to longitudinal polarization and unidirectional electric field the electric potential is expanded as function of longitudinal coordinate x.

3.4 Energies of the fluid flow

The fluid flow conditions are assumed to be fully developed, isentropic and irrotational. Due to irrotational condition, the scalar potential function, Ψ is defined so that the flow velocity vector is expressed as [15]:

$$\vec{V}_f = -\nabla\Psi \tag{12}$$

The function Ψ contains two parts: one of which is due to undisturbed mean flow velocity U_f in the axial direction and the other one is unsteady perturbation potential φ correspond to shell motions and distortions. Hence, the potential function can be expressed as:

$$\Psi = U_f x + \varphi \tag{13}$$

For modeling of the fluid flow behaviors, the cylindrical coordinates r, θ and z is used with the origin located at the center of shell's section. The components of the fluid velocities in cylindrical coordinates are given by

$$V_x = U_f + \frac{\partial\varphi}{\partial x},\ V_\theta = \frac{1}{r}\frac{\partial\varphi}{\partial\theta},\ V_r = \frac{\partial\varphi}{\partial r} \tag{14}$$

Using Bernoulli's equation for unsteady fluid flow, the perturbed pressure P can be related to potential of perturbation velocity as [8]:

$$\frac{\partial\varphi}{\partial t} + \frac{1}{2}V^2 + \frac{P}{\rho_f} = \frac{P_S}{\rho_f} \tag{15}$$

where ρ_f is fluid density. P_S is stagnation pressure and calculated as $P_S = \bar{P} + \frac{1}{2}\rho_f U_f^2$ [8]. The pressure P is composed of a mean pressure $\bar{P}$ and a perturbation pressure P_p assumed positive outward the shell as:

$$P = \bar{P} + P_p \tag{16}$$

Therefore, the perturbation pressure is obtained as [8]:

$$P_p = -\rho_f\left(\frac{\partial\varphi}{\partial t} + U_f\frac{\partial\varphi}{\partial x}\right) \tag{17}$$

Supposing that no cavitation occurs at the interface of shell and fluid, the boundary conditions for potential of perturbation velocity can be expressed as:

$$\left.\frac{\partial\varphi}{\partial r}\right|_{r=R} = \frac{\partial w}{\partial t} + U_f\frac{\partial w}{\partial x} \tag{18}$$

Applying method of separation of variables to φ, one can write

$$\varphi(x,r,\theta,t) = \sum_{m=1}^{M}\sum_{n=0}^{N}\Phi_m(x)\Xi_{m,n}(r)\cos(n\theta)f_{m,n}(t) \tag{19}$$

Using above equation and imposing regularity condition at $r=0$ for potential of perturbation velocity, the unknown functions in Eq. (19) are obtained as:

$$\begin{aligned} \Phi_m(x) &= \sin\left(\frac{m\pi x}{L}\right) \\ \Xi_{m,n}(r) &= I_n\left(\frac{m\pi r}{L}\right) \end{aligned} \tag{20}$$

where I_n is modified Bessel function of the first kind of order n.

The Eq. (19) must satisfy boundary condition (Eq. (18)), Hence Eq. (19) is rewritten as:

$$\phi(x,r,\theta,t) = \sum_{m=1}^{M}\sum_{n=0}^{N} \frac{L}{m\pi} \frac{I_n(m\pi r/L)}{I'_n(m\pi R/L)} \left(\frac{\partial w}{\partial t} + U_f \frac{\partial w}{\partial x}\right) \tag{21}$$

where I'_n is first derivative of I_n.

The total energy associated with the fluid flow is defined as [8]:

$$E_F^T = \frac{1}{2}\rho_f \iiint_\Gamma \vec{V}_f . \vec{V}_f \, d\Gamma \tag{22}$$

where Γ is the cylindrical fluid volume inside the shell. Based on Green's theory, Eq. (22) can be expressed as:

$$\begin{aligned} E_F^T &= E_F^p + \frac{1}{2}\rho_f \int_0^{2\pi}\int_0^L \left(U_f x \frac{\partial \varphi}{\partial r}\right)_{r=R} dxRd\theta \\ &+ \frac{1}{2}\rho_f \int_0^{2\pi}\int_0^R \left(U_f L \frac{\partial \varphi}{\partial x}\right)_{x=L} rdrd\theta \\ &+ \frac{1}{2}\rho_f U_f^2 \pi R^2 L, \end{aligned} \tag{23}$$

where E_F^p is the energy of fluid respect to potential of perturbation velocity and is expressed as:

$$E_F^p = \frac{1}{2}\rho_f \int_0^{2\pi}\int_0^L \left(\varphi \frac{\partial \varphi}{\partial r}\right)_{r=R} dxRd\theta \tag{24}$$

Substituting Eq. (18) into Eq. (24), following equation is obtained

$$\begin{aligned} E_F^p &= \frac{1}{2}\rho_f \int_0^{2\pi}\int_0^L \sum_{m=1}^{M}\sum_{n=0}^{N} \frac{L}{m\pi} \frac{I_n(m\pi R/L)}{I'_n(m\pi R/L)} \\ &\times \left[\dot{w}^2 + U_f\left(\dot{w}\frac{\partial w}{\partial x}\right)^2 + U_f^2\left(\frac{\partial w}{\partial x}\right)^2\right] dxRd\theta. \end{aligned} \tag{25}$$

3.5 Effect of fluid viscosity

In this study, the viscosity effect of fluid is considered as an external force. Hence the time-mean Navier–Stokes equations for a fully developed turbulent, incompressible axial flow are expressed as [8]:

$$\begin{aligned}
&\frac{1}{\rho_f}\frac{\partial P}{\partial x} = -\frac{1}{r}\frac{d}{dr}\left(r\bar{u}_x\bar{u}_r\right) + \frac{\eta}{r}\frac{d}{dr}\left(r\frac{dU_f}{dr}\right)\\
&\frac{1}{\rho_f}\frac{\partial P}{\partial r} = -\frac{1}{r}\frac{d}{dr}\left(r\bar{u}_r^{\,2}\right) + \frac{\bar{u}_\theta^{\,2}}{r}\\
&0 = \frac{d}{dr}\left(\bar{u}_r\bar{u}_\theta\right) + 2\frac{\bar{u}_r\bar{u}_\theta}{r}
\end{aligned} \tag{26}$$

where over-bar denotes time-mean, η kinematic viscosity and $\bar{u}_x$, $\bar{u}_\theta$, $\bar{u}_r$ are fluctuating velocities in the axial, circumferential and radial directions, respectively. Pressure distribution can be estimated by using computational fluid dynamics (CFD) as [16]:

$$P\left(x,r\right) = -2\frac{\rho_f}{R}U_\tau^2 x - \rho_f\bar{u}_r^{\,2} + \rho_f\int_R^r \frac{\bar{u}_\theta^{\,2} - \bar{u}_r^{\,2}}{r}dr + P\left(0,R\right) \tag{27}$$

in which the stress velocity U_τ is defined as:

$$U_\tau = \left(-\eta\frac{dU_f}{dr}\right)_{r=R}^{1/2} = \left(\frac{\tau_W}{\rho_f}\right)^{1/2} = \left(\frac{1}{8}fU_f^2\right)^{1/2} \tag{28}$$

where τ_W and f are the fluid frictional force per unit area on the shell and the friction factor respectively.

The pressure distribution on the shell's interface can be written as:

$$P\left(x,R\right) = -2\frac{\rho_f}{R}U_\tau^2 x + P\left(0,R\right) = -\frac{\rho_f}{4R}fU_f^2 x + P\left(0,R\right) \tag{29}$$

Now, the longitudinal pressure drop in the shell can be expressed as:

$$\Delta P = P(0,R) - P(L,R) = 2\frac{\rho_f}{R}U_\tau^2 L = \frac{\rho_f}{4R}fU_f^2 L \tag{30}$$

The friction factor f in Eqs. (28 to 30) is evaluated by the empirical Colebrook equation as [15]:

$$\frac{1}{\sqrt{f}} + 2\log\left(\frac{\delta/2R}{3.7} + \frac{2.51}{\mathrm{Re}\sqrt{f}}\right) = 0 \tag{31}$$

where δ is average height of surface roughness of the shell and Re is the Reynolds number introduced by $\mathrm{Re} = 2RU_f/\eta$.

The viscosity effect is due to longitudinal pressure drop on the interface of fluid-shell and the distributed axial load exerted on the shell surface. The work done due to viscosity effect is calculated as:

$$W^{Fluid\ Viscosity} = \int_0^{2\pi}\int_0^L \left(\Delta Pw + \tau_W u\right)dxRd\theta \tag{32}$$

Using Lagrange motion equations, governing equations are solved by Rayleigh–Ritz method and the results discussed in the next section.

4 NUMERICAL RESULTS AND DISCUSSION

The structural properties of Poly-Vinylidene fluoride (PVDF) are given in Table 1.[18].

Table 1
Properties of PVDF.

Properties	PVDF [18]	Properties	PVDF [18]
C_{11} (GPa)	238.24	e_{31} (C/m^2)	–0.13
C_{22} (GPa)	23.6	e_{32} (C/m^2)	–0.145
C_{33} (GPa)	10.64	e_{33} (C/m^2)	–0.276
C_{12} (GPa)	3.98	e_{24} (C/m^2)	–0.009
C_{13} (GPa)	2.19	e_{15} (C/m^2)	–0.135
C_{23} (GPa)	1.92	$\in_0$ (F/m)	8.854185×10^{-12}
C_{44} (GPa)	2.15	$\in_{11}/\in_0$	12.5
C_{55} (GPa)	4.4	$\in_{22}/\in_0$	11.98
C_{66} (GPa)	6.43	$\in_{33}/\in_0$	11.98

In order to validate present study, a simplified case of the analysis is considered by neglecting piezoelectric characteristic and micro-scaling of the tube. The results presented by Amabili et al. [16] are compared with the results of this investigation, in Fig. 2 which shows a very good agreement between them.

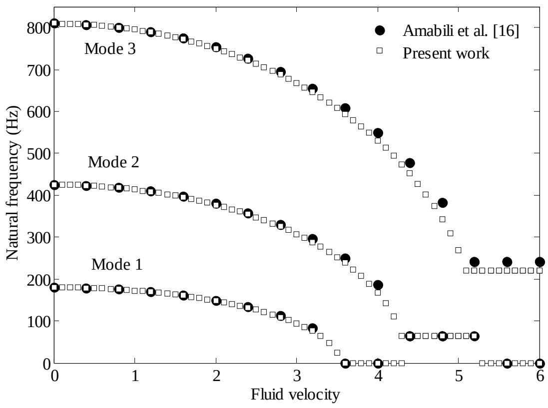

Fig.2
Comparison between present results with those presented by Amabili et al. [16].

In order to study effect of flow velocity and elastic medium, dimensionless parameters are defined as follow:

$$\Omega^* = \Omega L\sqrt{\rho_s / C_{11}},\ U_f^* = U_f\sqrt{\rho_f / C_{11}}$$
$$K_W^* = K_W / C_{11},\ G_P^* = G_P / C_{11}Rh \tag{33}$$

Fig. 3 shows the dimensionless natural frequency of the 1st mode with varying dimensionless flow velocity for different magnitudes of dimensionless small scale parameter $e_0 a / L$. It is found that increasing small scale parameter leads to decrease frequency in different fluid velocities and has major effect on critical flow velocity.

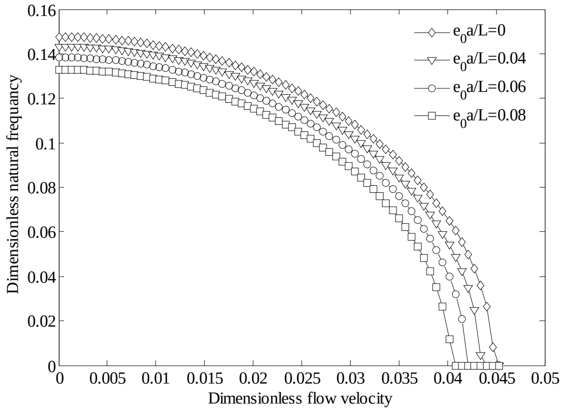

Fig.3
Effect of small-scale parameter on natural frequency with changing fluid velocity.

Figs. 4 and 5 indicate dimensionless natural and damping frequencies versus dimensionless flow velocity respectively for different vibration mode. It is observed that for first mode, system is fallen into instability (real part of Ω^* becomes non-zero) when the dimensionless flow velocity is within the range $0.045 < U_f^* < 0.09$. For range $0.12 < U_f^* < 0.14$, instability occurs for second mode while the natural frequencies for the first and second modes have been merged to same value. This process is similarly repeated for the next modes with increasing flow velocity.

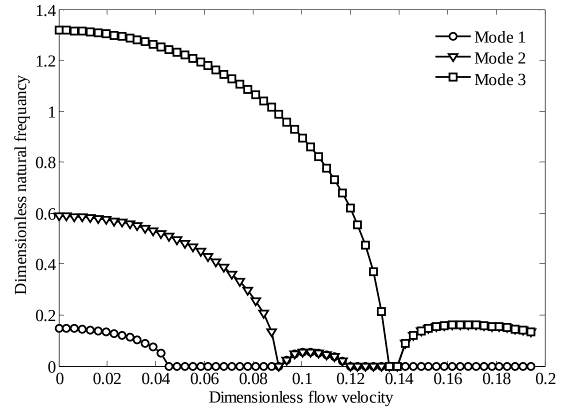

Fig.4
Dimensionless natural frequencies versus dimensionless fluid velocity for 1st to 4th mode.

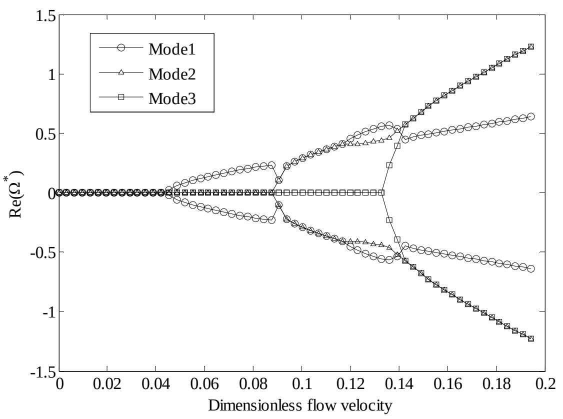

Fig.5
Dimensionless damping frequencies versus dimensionless fluid velocity for 1st to 4th mode.

The qualitative investigation on effect of surrounding media and comparison between Winkler and Pasternak models are illustrated in Fig. 6. This Figure shows that elastic medium causes to increase natural frequency and the stability of the system and Pasternak foundation is more effective than Winkler in this regard.

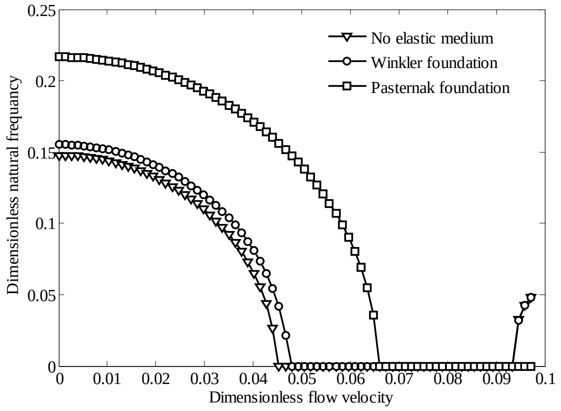

Fig.6
Effect of elastic medium model on natural frequency with changing fluid velocity.

The effects of Winkler and Pasternak modulus are shown in Figs. 7 and 8. As can be predicted, the dimensionless natural frequency is increased with increasing modulus of elastic medium. For the Winkler model the natural frequency is increasing with a decreasing rate with respect to Winkler modulus, while for the case of Pasternak model the natural frequency is increasing almost with a constant rate for lower flow velocities.

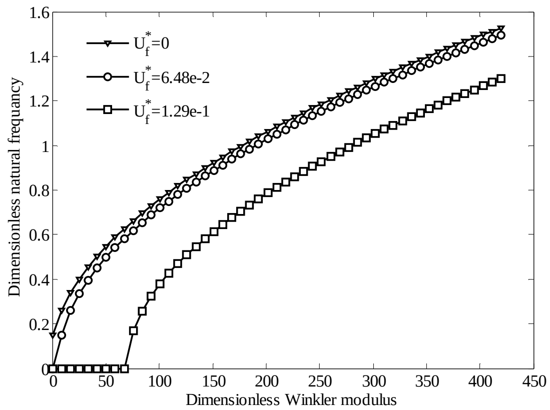

Fig.7
Dimensionless natural frequency versus dimensionless Winkler modulus for various fluid velocities.

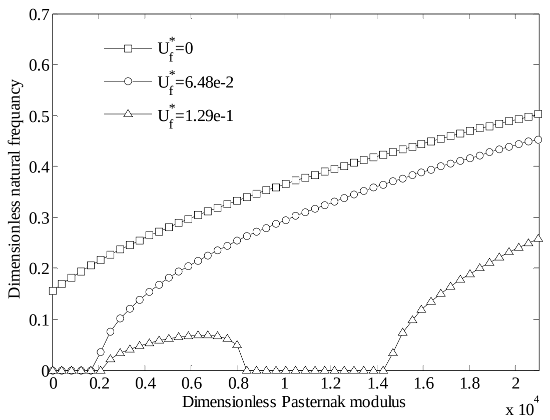

Fig.8
Dimensionless natural frequency versus dimensionless Pasternak modulus for various fluid velocities.

Effect of temperature change on dimensionless natural frequency of the system is illustrated in Fig. 9. It can be concluded that temperature rise decreases nonlinear frequency. With increasing flow velocity, the nonlinearity effect becomes much more significant. Therefore the effect of temperature change becomes considerable by increasing flow velocity.

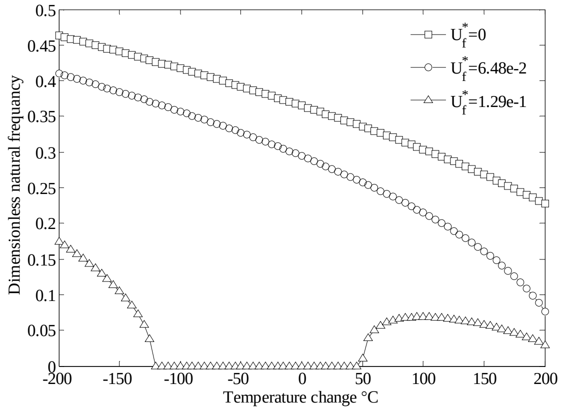

Fig.9
Dimensionless natural frequency versus temperature change for various fluid velocities.

The effect of fluid viscosity is demonstrated in Fig. 10. It can be observed that the influence of viscosity becomes significant when the flow velocity is increased and critical flow velocity is diminished when the viscosity of fluid is ignored.

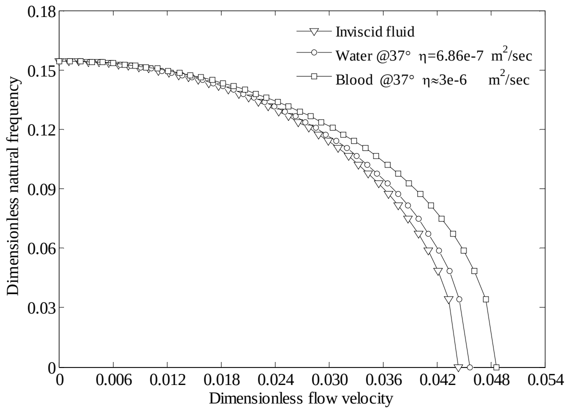

Fig.10
Effect of fluid viscosity on natural frequency with changing fluid velocity.

The frequency ratio versus flow velocity for different values of small scale parameter is shown in Fig. 11. It is concluded that nonlinearity effects are increased with increasing flow velocity. In other word, linear approximation in the analysis can be employed only for lower fluid velocities.

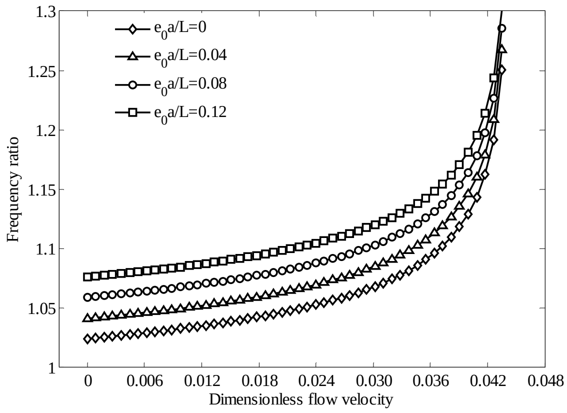

Fig.11
Frequency ratio versus dimensionless fluid velocity for different values of small scale parameter.

Fig.12 indicates frequency ratio versus aspect ratio of the micro-tube. It is found that for higher aspect ratios the linear analysis can be used with appropriate accuracy but for lower ones, the effect of nonlinearity on the results is considerable and cannot be ignored.

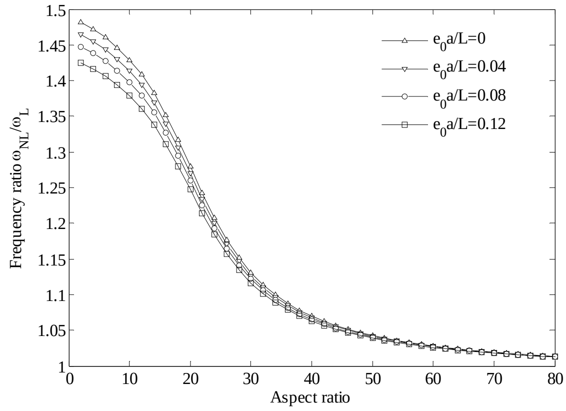

Fig.12
Frequency ration versus aspect ratio for different values of small scale parameter.

Variation of natural frequency with respect to flow velocity for different values of the imposed electric potential is illustrated in Fig. 13. It is concluded that the positive imposed electric potential increases the stability of the system which can be used to control the vibration response of the micro-tube.

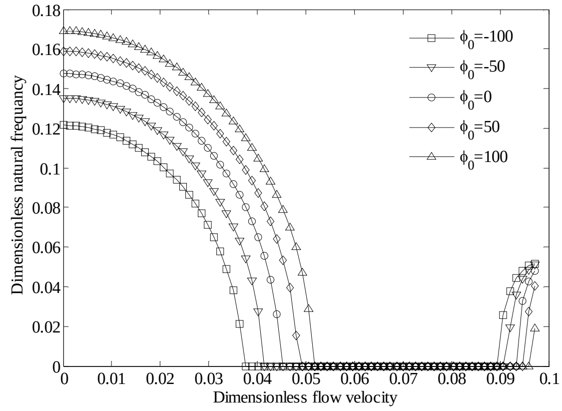

Fig.13
Dimensionless natural frequency versus fluid velocity for various magnitudes of imposed electric potential.

The piezoelectric responses of the smart micro-tube are demonstrated in Figs. 14and 15. The electric potential distributions along the micro-tube for various small scale parameters are shown in Fig. 14. It can be seen from this figure that increasing small scale parameter causes to decrease magnitudes of induced electric potential. Fig. 15 shows the distribution of electric potential along the micro-tube with varying flow velocity. Increasing velocity of fluid from zero to critical value, leads to increasing magnitudes of induced electric potential.

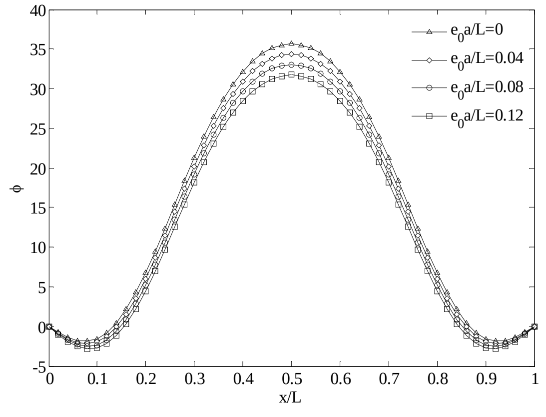

Fig.14
Distribution of electric potential along micro-tube for different values of small scale.

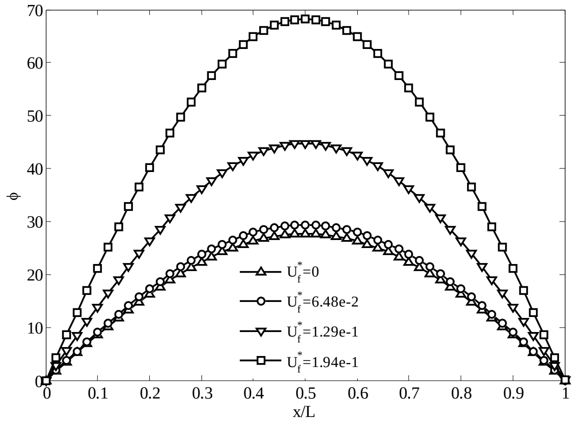

Fig.15
Distribution of electric potential along micro-tube for different values of fluid velocity.

6 CONCLUSIONS

General theoretical analysis of electro-thermo-mechanical nonlocal nonlinear vibration of piezoelectric micro-tube conveying fluid made of PVDF is developed in this study. This smart structure embedded in an elastic medium as Pasternak foundation which is considering shear effect. Higher order governing equations were solved by Ritz method.

Regarding fluid flow effects, it has been concluded that the fluid flow is basically an effective factor on decreasing natural frequency leading to instability of the micro-tube. Also, it has been found that the stability of the system is strongly dependent on the imposed electric field so that increasing the imposed positive electric potential significantly increases the stability of the system. As a most important result of this study, the imposed electric potential and the uniform thermal fields are the effective parameters in order to control the response of this kind of hydraulic sensors and actuators.

ACKNOWLEDGMENTS

The authors are grateful to University of Kashan for supporting this work by Grant No. 65475/28. They would also like to thank the Iranian Nanotechnology Development Committee for their financial support. This research was supported by the Thermoelasticity Center of Excellence, Mechanical Engineering Department, Amirkabir University of Technology.

REFERENCES

[1] Salehi-Khojin A., Jalili N., 2008, Buckling of boron nitride nanotube reinforced piezoelectric polymeric composites subject to combined electro-thermo-mechanical loadings, *Composites Science and Technology* **68**(6):1489-1501.

[2] Ghorbanpour Arani A., Amir S., Shajari A.R., Mozdianfard M.R., Khoddami Maraghi Z., Mohammadimehr M.,2011, Electro-thermal non-local vibration analysis of embedded DWBNNTs, *Proceedings of the Institution of Mechanical Engineers, Part C: Journal of Mechanical Engineering Science* **226**(5) :1410-1422.

[3] Ghorbanpour Arani A., Amir S., Shajari A.R., Mozdianfard M.R., 2012, Electro-thermo-mechanical buckling of DWBNNTs embedded in bundle of CNTs using nonlocal piezoelasticity cylindrical shell theory, *Compos. Part B: Engineering* **43**(2):195-203.

[4] Ghorbanpour Arani A., Shokravi M., Amir S., Mozdianfard M.R., 2012, Nonlocal electro-thermal transverse vibration of embedded fluid-conveying DWBNNTs, *Journal of Mechanical Science and Technology* **26**(5):1455-1462.

[5] Shu C., 1996, Free vibration analysis of composite laminated conical shells by generalized differential quadrature, *Journal of Sound and Vibration* **194**(3): 587-604.

[6] Rahmani O., Khalili S.M.R., Malekzadeh K., 2009, Free vibration response of composite sandwich cylindrical shell with flexible core, *Composite Structures* **92**(5):1269–1281.

[7] Amabili M., Pellicano F., Païdoussis M.P., 1999, Non-linear dynamics and stability of circular cylindrical shells containing flowing fluid. Part I: stability, *Journal of Sound and Vibration* **225**(4): 655–699.

[8] Ghorbanpour Arani A., Shajari A.R., Amir S., Loghman A.,2013, Electro-thermo-mechanical nonlinear nonlocal vibration and instability of embedded micro-tube reinforced by BNNT conveying fluid, *Physica E* **45**:424-432.

[9] Yang J., 2005, An Introduction to the Theory of Piezoelectricity, Springer, Lincoln, Ninth Edition.

[10] Eringen A.C., 1983, On differential equations of nonlocal elasticity and solutions of screw dislocation and surface waves, *Journal of Applied Physics* **54**(9): 4703–4710.

[11] Amabili M., 2008, Nonlinear Vibrations and Stability of Shells and Plates, Cambridge University Press, Parma, First Edition.

[12] Ghorbanpour Arani A., Zarei M.S., Mohammadimehr M., Arefmanesh A., Mozdianfard M.R., 2011, The thermal effect on buckling analysis of a DWCNT embedded on the Pasternak foundation, *Physica E* **43**(9): 1642–1648.

[13] Kurylov Ye., Amabili M., 2010, Polynomial versus trigonometric expansions for nonlinear vibrations of circular cylindrical shells with different boundary conditions, *Journal of Sound and Vibration* **329**(9): 1435–1449.

[14] Alinia M.M., Ghannadpour S.A.M., 2009, Nonlinear analysis of pressure loaded FGM plates, *Composite Structures* **88**(3): 354–359.

[15] Fox R.W., Pritchard P.J., McDonald A.T., 2008, Introduction to Fluid Mechanics, Wiley, New York, Forth Edition.

[16] Amabili M., Karagiozis K., Païdoussis M.P., 2009, Effect of geometric imperfections on non-linear stability of circular cylindrical shells conveying fluid, *International Journal of Non-Linear Mechanics* **44**(3): 276 – 289.

[17] Yang J., Ke L.L., Kitipornchai S., 2010, Nonlinear free vibration of single-walled carbon nanotubes using nonlocal Timoshenko beam theory, *Physica E* **42**(5): 1727–1735.

[18] Cheng Z.Q., Lim C.W., Kitipornchai S., 2000, Three-dimensional asymptotic approach to inhomogeneous and laminated piezoelectric plates, *International Journal of Solids and Structures* **37**(23): 3153–3175.